A novel approach to statistical-dynamical downscaling for long-term wind resource predictions

Article

Accepted Version

A novel approach to statistical-dynamical downscaling for long-term wind resource predictions

Journal:	*Meteorological Applications*
Manuscript ID	MET-16-0155.R1
Wiley - Manuscript type:	Research Article
Date Submitted by the Author:	n/a
Complete List of Authors:	Chávez-Arroyo, Roberto; Tecnológico de Monterrey, Escuela de Ingeniería y Ciencias; Centro Nacional de Energias Renovables, Energía Eólica Fernandes-Correia, Pedro; Centro Nacional de Energias Renovables, Energía Eólica Lozano-Galiana, Sergio; Centro Nacional de Energias Renovables, Energía Eólica Sanz-Rodrigo, Javier; CENER, Wind energy department Amezcua, Javier; University of Reading, Department of Meteorology Probst, Oliver; Tecnológico de Monterrey, Escuela de Ingeniería y Ciencias
Keywords:	Energy < Climate change impacts, NWP < Modelling, Sensitivity Analysis < Modelling, Statistical Models < Modelling, Reliability < Verification, Ensemble < Climate change impacts
Manuscript keywords:	Long-term wind resource, statistical-dynamical downscaling, stratified sampling, mean sea level maps, image processing, reanalysis data

Graphical table of contents

A novel approach to statistical-dynamical downscaling for long-term wind resource predictions

Roberto Chávez-Arroyo, Pedro Fernandes-Correia, Sergio Lozano-Galiana, Javier Sanz-Rodrigo, Javier Amezcua, *Oliver Probst

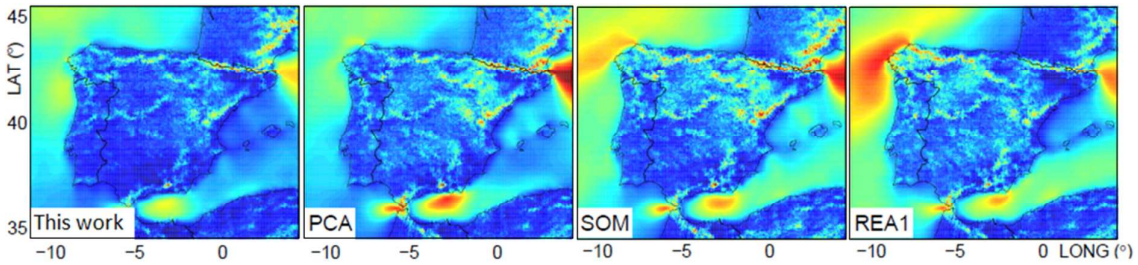

A novel method to determine representative periods (typically a year) for the estimation of the long-term mesoscale wind resource has been proposed and compared to other recently published techniques. It provides a computationally lean while accurate solution of the problem of constructing long-term mesoscale wind maps through downscaling without having to go through a *brute force* procedure. Applications include a wider dissemination of mesoscale wind maps because of faster and cheaper execution, as well as greater flexibility for sensitivity analyses.

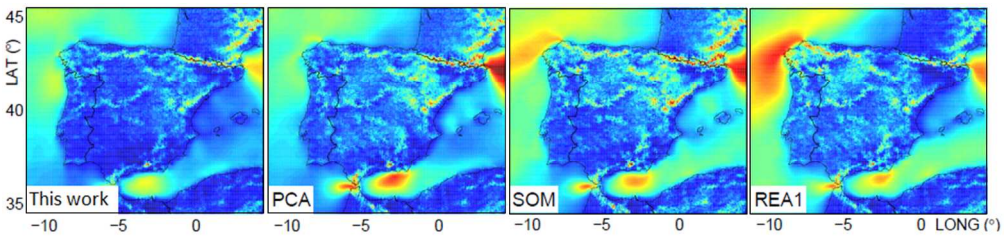

781x184mm (96 x 96 DPI)

A novel approach to statistical-dynamical downscaling for long-term wind resource predictions

[1,2]Roberto Chávez-Arroyo, [2]Pedro Fernandes-Correia, [2]Sergio Lozano-Galiana, [2]Javier Sanz-Rodrigo, [3]Javier Amezcua, [1,*]Oliver Probst

[1]School of Engineering and Sciences, Tecnológico de Monterrey, Eugenio Garza Sada 2501 Sur, Monterrey, NL, CP 64849, Mexico; [2]Centro Nacional de Energías Renovables, Av. Ciudad de la Innovación, 7, 31621 Sarriguren, Navarra, Spain; [3]Department of Meteorology, University of Reading, Earley Gate, PO Box 243, Reading, RG6 6BB, UK

*Corresponding author: oprobst@itesm.mx

Abstract

A new method for the long-term prediction of the wind resource based on the concept of statistical-dynamical downscaling is presented. This new approach uses mean sea-level pressure (MSLP) maps from global reanalysis data (NCEP-DOE AMIP-II) and image processing techniques to identify a synthetic reference period which optimally matches the corresponding long-term maps. Four different image processing techniques, averaged into one image similarity error index, are used to evaluate image similarity. A representative set of days is selected by requiring the error index to be minimal. Validation of representativeness in terms of the wind resource for the Iberian domain is performed against ten years of measured wind data from Navarra (Spain), as well as mesoscale simulations of the Iberian Peninsula. The new approach is shown to outperform not only the industry-standard method but also other recently proposed methods in its capability to achieve mesoscale level representativeness. A particular advantage of the new method is its capability of simultaneously providing a representative period for all potential wind farm sites located within large regional domains without requiring re-running the method for different candidate sites.

Keywords: Long-term wind resource; statistical-dynamical downscaling; stratified sampling; mean sea level maps; reanalysis data; image processing

1. Introduction

The accurate representation of large-scale circulation systems and their associated local wind field is essential to the development and financing of wind power plants. Consequently, the interest in methods providing insights into the representativeness of on-site measured wind data has sparked in recent years. To date, most industry-standard analyses of the long-term wind resource of a wind project rely on statistical relationships (Romo Perea *et al.*, 2011), often in the form of a linear regression, between the on-site towers and suitable reference sites, typically either Automatic Surface Observation Stations (ASOS) or virtual wind towers from numerical climate data bases such as NCEP/NARR (North American Regional Reanalysis) (Mesinger *et al.*, 2006), NASA/MERRA (Modern-Era Retrospective Analysis for Research and Applications) (Rienecker *et al.*, 2011), ECMWF/ERA-Interim among others (Liléo *et al.*, 2013). While the predictions derived from statistical relationships may be quite accurate if the long-term station is located at a site with similar wind climate and exposure conditions, and long-term measurements have been conducted at a height level similar to the projected turbine hub height, these idealized conditions are only seldom met. The construction of statistical associations between long-term

atmospheric data with local variables is widely known as *statistical downscaling*. In these methods, a statistical model is trained to use empirical relationships between local observed variables, predictands, and large scale atmospheric fields known as predictors (e.g. García-Bustamante *et al.* (2012)). This approach is very computationally efficient; however, similar to the virtual series method, its reliability relies on the strength of the statistical links between atmospheric circulations and regional observations.

On the opposite side are approaches that solve the equations of the atmosphere dynamics for a period of interest. Such approaches are generally referred to as *dynamical downscaling* and provide solutions to the atmospheric dynamics in the region of interest based on the full set of balance equations at the chosen simulation grid and semi-empirical relationships for physical processes occurring at the sub-grid level (Pielke, 2002). A possible approach to assessing the long-term wind resource in a region of interest is to apply the dynamical downscaling methodology for periods long enough to capture the intra- and inter-annual, and if possible, decadal variability. Despite the significant increase in computing power, the need for solutions at finer-resolution scales and the continuous development of more complex physics such as the implementation of higher-order models for the solution of sub-grid processes (e.g. Barranger & Kallos (2012)) requires substantially higher computational resources than those typically available at the desktop level or in small research clusters.

Practical solutions to the dilemma outlined above are *hybrid methods*, often termed *statistical dynamical downscaling* (SDD), which combine the deterministic approach of dynamical downscaling with statistical techniques. SDD methods can be roughly grouped into three categories: (1) approaches based on the classification of weather types (Frey-Buness *et al.*, 1995), (2) algorithmic methods with suitable evaluation metrics where almost no pre-classification by the user is required (Fuentes & Heimann, 2000a; Cutler *et al.*, 2006; Hagemann, 2008; Rife *et al.*, 2013; Tammelin *et al.*, 2013; Chávez-Arroyo *et al.*, 2013; Martinez *et al.*, 2013), and (3) construction of statistical relations between long-term and short-term dynamical downscaled data (Hahmann *et al.*, 2012). Weather classification approaches are rather typical in the atmospheric sciences, where algorithmic methods have made a more recent appearance. In both cases the underlying assumption is that any regional climate can be associated with a specific frequency distribution of classified large-scale weather situations (Frey-Buness *et al.*, 1995).

While methods based on the synoptic-scale classification of stationary weather regimes are generally physically meaningful and often lead to a reasonably small number of classes, there are several downsides which limit their usefulness for comprehensive wind prospecting purposes. First, there is generally a loss of the time-dependent phenomena (Fuentes & Heimann, 2000b). Secondly, the simulation of daily or seasonal phenomena is difficult because of the large number of classes required for such a distinction. Thirdly, classification is rather case-specific and somewhat subjective as it requires site-specific knowledge (Cutler *et al.*, 2006).

Some of these issues can in principle be tackled by algorithmic approaches such as those described below. Martínez et al. (2013) disaggregated the large-scale climate into their Empirical Orthogonal Functions (EOF) which were then dynamically downscaled. They were able to account for the temporal variability by applying the Principal Components time series to the downscaled version of the corresponding EOF which also served for the comparisons with observations. Fuentes and Heimann (2000) proposed the dynamical downscaling of the most representative multi-day episodes of quasi-stationary circulations. These episodes were created by hierarchical cluster analysis combined with a spatio-temporal metric to collect consecutive dates with similar patterns described by their first Principal Components of the geopotential at 500 hPa. Hagemann (2008) proposed the use of Self-Organizing Maps

(SOM) to select a representative continuous set of 365 days which were afterwards dynamically downscaled.

Rife et al. (2013) based their selection on a 365-day sample with equal representation for all days. The sample resulted from testing very large number sets generated by random stratified sampling and selecting the best rated sample's wind speed and direction distributions according to their proposed distance metric based on the χ^2 statistic. Their selection was made from daily averages of wind speed and direction from the first native vertical level from the MERRA global reanalysis data point that best correlated with the measurements used for validation. The ideas of Hageman (2008), Tammelin *et al.* (2013) and Rife *et al.* (2013) were also addressed by Chavez-Arroyo *et al.* (2013) and Chávez-Arroyo *et al.* (2015). They employed the stratified sampling technique (Rife *et al.*, 2013) to generate a large pool of candidate years that were ranked according to their similarity to the long-term climate. Chávez-Arroyo *et al.*(2013), Chávez-Arroyo *et al.* (2015), and (Hagemann (2008) used large-scale atmospheric circulation predictors, which probe representativeness at a mesoscale level. Recently, Vanvyve *et al.* (2015) presented another interesting methodology suitable for statistical-dynamical downscaling based on an analogue ensemble approach.

The present work is a new contribution to the field of statistical dynamical downscaling and has two main objectives: (1) introduction of an improved algorithmic approach for the determination of representative periods, and (2) a systematic comparison of the new proposal against published methods. The new method is based on the assumption that regional wind flow is driven by large-scale systems which can be suitably analysed in terms of synoptic patterns. While the previously published methods require a relatively modest computing time compared to the one required for downscaling large regional areas the computational effort is still considerable, which motivated the search for a computationally leaner method which should ideally retain or improve the accuracy of the previously proposed methods for identifying representative periods. As will be shown in the following, the novel approach proposed in this work does indeed comply with these expectations.

2. Methods and data

A total of five different methods for the determination of representative periods were evaluated. One technique, termed the *Best Annual Mean and Standard Deviation* or BAMS method, is new and will be described at some detail in the present paper. It will be shown that this novel approach consistently outperforms all other methods. Another important method implemented and evaluated in this work is the one put forward by Rife *et al.* (2013) discussed above. The Rife method was implemented in two variants (REA1 and REA2) described in greater detail below. Two other techniques recently published and used for comparison in the present work are the PCA (Principal Component Analysis)-based approach proposed by Chávez-Arroyo *et al.* (2013) and the SOM (Self-Organizing Maps) method used by Chávez-Arroyo *et al.* (2015). The last method used for comparison and termed the traditional (TRA) approach in this work is the wind industry-standard procedure for statistical downscaling of the long-term wind resource. The traditional method (TRA) is based on the construction of one synthetic year (365 days) where each calendar day of the representative year is determined from random draws among the corresponding set of repetitions of that calendar day within the long-term period.

2.1 The Best Annual Mean and Standard Deviation (BAMS) method

The novel approach introduced in this work incorporates several elements explored successfully in published work. One key ingredient is the use of mean sea-level pressure (MSLP) mesoscale maps for a

region of interest as predictors; this approach was found to outperform the industry-standard practice in Chávez-Arroyo *et al.* (2013) and Chávez-Arroyo *et al.* (2015). Another element is the use of the stratified sampling technique put forward by Rife *et al.* (2013) in which a large number of monthly data sets (10^5 samples/month) are generated by randomly sampling the long-term SLP data, each sample containing 28, 30, or 31-days per month, depending on the calendar month. The new ingredient in the BAMS method is the way the similarity between the long-term and the representative period is established. Whereas Rife *et al.* (2013) use comparisons between wind resource at a point location the BAMS method uses a mesoscale approach to establish this similarity by using the complete information contained in the regional MSLP maps. Such an approach seems more appropriate for mesoscale downscaling applications, though it was clear from the outset that the Rife approach might work better at the specific location used for tuning the method.

Evidently, a tool is required to establish the similarity between mesoscale maps. The novelty in the present work consists in its departure from traditional statistical methods used in the atmospheric sciences, both linear (such as PCA) and non-linear (such as SOM), by using image processing techniques successfully employed in other areas of science and engineering. Four different image similarity detection techniques are used and combined into one similarity index after applying a linear normalization operator to the sub-index associated with each method. An optimal or representative set of days is selected by requiring the error index to be minimal.

In the following we will consider two types of maps, $L(s)$ (long-term) and $R(s)$ (candidate representative period), which have been obtained from temporally averaging over their respective observational periods; $s \in [1, Q]$ with Q being the number of grid points. Both the temporal mean (e.g. $L(s) = \sum L(s,t)/T$) and the standard deviation (e.g. $L(s) = (\sum (L(s,t) - \bar{L})^2)^{1/2}/(T-1)$ are considered for both of the similarity indices considered. We can then define the *first similarity index* SI_1 as the root mean square error of the point-to-point comparison between the L and R map as

$$\mathrm{SI}_1 \equiv \langle \varepsilon \rangle = \left(\frac{1}{Q} \sum_{r=1}^{Q} (L_r - R_r)^2 \right)^{1/2} \tag{1}$$

The *second similarity index* SI_2 is an average Pearson correlation coefficient $\rho(x, y)$ between rows and columns from each pair of maps. In order to account for small variations in the sea level pressure (SLP) patterns which are due to small shifts between maps but still represent almost identical spatial patterns, the correlations are computed not only between corresponding rows (i.e., $\rho(R_a, L_a)$, a being the row index, $a \in [1, A]$, A being the number of rows) and columns (i.e. $\rho(R_b, L_b)$, b being the column index, $b \in [1, B]$), B being the number of columns), but also from certain neighbouring rows and columns as defined by $\rho(R_a, L_{a \pm 0.03A})$ and $\rho(R_b, L_{b \pm 0.03B})$, respectively, i.e.

$$\mathrm{SI}_2 \equiv \bar{\rho} = \frac{1}{3A} \sum_{k=-1}^{1} \sum_{a=1}^{A} \rho(R_a, L_{a+k\ 0.03A}) + \frac{1}{3B} \sum_{k=-1}^{1} \sum_{b=1}^{B} \rho(R_b, L_{b+k\ 0.03B}) \tag{2}$$

The third similarity index $\mathrm{SI}_3 = \gamma$, is based on a comparison between distributions of the SLP values contained in both rows and columns of the images representing the long-term and the candidate representative period, respectively. As before, the analysis is conducted on both the average SLP and its standard deviation. Specifically, the following calculations are carried out: a histogram f_a of the SLP

values of the ath row and, similarly, a histogram g_b of the SLP values of the bth column in each of the SLP mean or standard deviation map is first calculated using 30 bins. Then, the Pearson correlation for all pairs of distributions is calculated from the rows with the same index, i.e. corr$(f_a^{\mathrm{LT}}, f_a^{\mathrm{RP}})$ and, similarly, from columns with the same index, i.e. corr$\left(g_b^{\mathrm{LT}}, g_b^{\mathrm{RP}}\right)$, where in both cases the superscript LT refers to *long-term* and RP to *representative period*. Finally the row and column correlations are averaged to compute the third similarity index γ according to

$$\mathrm{SI}_3 \equiv \gamma = \frac{1}{A+B}\left(\sum_{a=1}^{A} \mathrm{corr}(f_a^{\mathrm{LT}}, f_a^{\mathrm{RP}}) + \sum_{b=1}^{B} \mathrm{corr}\left(g_b^{\mathrm{LT}}, g_b^{\mathrm{RP}}\right)\right) \tag{3}$$

The fourth metric or similarity index SI_4 is a structural similarity index proposed by Wang *et al.* (2004). This technique is designed for the quality assessment based on the degradation of structural information of an image. This technique attempts to quantify the visibility of errors (differences) between a distorted image and a reference image. The structural similarity index SSIM for two images x and y is computed as:

$$\mathrm{SI}_4 \equiv \mathrm{SSIM}(x,y) = \left[l(x,y)^{\alpha} c(x,y)^{\beta} s(x,y)^{\Gamma}\right], \tag{4a}$$

where $l(x,y)$ is the luminosity function, $c(x,y)$ the contrast comparison function, and $s(x,y)$ the structure comparison function, respectively defined by

$$l(x,y) = \frac{2\mu_x\mu_y + C_1}{\mu_x^2+\mu_y^2 + C_1} \tag{4a}$$

$$c(x,y) = \frac{2\sigma_x\sigma_y + C_2}{\sigma_x^2+\sigma_y^2 + C_2} \tag{4b}$$

$$s(x,y) = \frac{\sigma_{xy} + C_3}{\sigma_x\sigma_y + C_3} \tag{4c}$$

The mean μ and the standard deviation σ of an image have their usual meanings, $\sigma_{xy} = \mathrm{cov}(x,y)$ is the covariance between images x and y, and C_1, C_2, and C_3 are small constants ($C_1 \ll \mu_x^2$, etc.). α, β, and Γ are free parameters used to adjust the relative importance of the three image comparison functions introduced above; in the present work $\alpha = \beta = \Gamma = 1$.

In the BAMS method, the four image similarity components described above are linearly transformed using the lower and upper bounds of each statistic calculated from the N samples making up the candidate set of representative periods i. This transformation scales the ranges of each of the four similarity indices to [0, 1] in order to allow them to be averaged into one overall similarity measure. The linearly scaled version $\phi_{i,j}^*$ of any of the four metrics ($\mathrm{SI}_k, k = 1 \ldots 4$) is then obtained from

$$\phi_{i,j}^* = \frac{\phi_{i,j} - \min_k\{\phi_{k,j}\}}{\max_k\{\phi_{k,j}\} - \min_k\{\phi_{k,j}\}}, \tag{5}$$

for the ith candidate and a given month j. All four normalized metrics are then averaged into one performance index $\tau_{i,j}$. In the present work, equal weights were assigned to the each of the four indices, although generalization to non-equal weights is evidently straightforward:

$$\tau_{i,j} = \frac{1}{4}\left\{\langle\varepsilon\rangle^*_{i,j} + \left(1 - \varrho^*_{i,j}\right) + \left(1 - \gamma^*_{i,j}\right) + \left(1 - \mathrm{SSIM}^*_{i,j}\right)\right\}, \tag{6}$$

where $\langle\varepsilon\rangle^*_{i,j}$, $\varrho^*_{i,j}$, $\gamma^*_{i,j}$, and $\mathrm{SSIM}^*_{i,j}$ are the linearly scaled versions of the four similarity indices according to equation (5). Please note that the complements of $\varrho^*_{i,j}$, $\gamma^*_{i,j}$, and $\mathrm{SSIM}^*_{i,j}$ are used in equation (6) are used for consistency with the first similarity metric $\langle\varepsilon\rangle^*_{i,j}$. The BAMS index is now constructed by averaging the performance indices $\tau_{i,j}$ for the monthly mean μ_{SLP} of the sea level pressure (SLP) and its standard deviation σ_{SLP}.

$$\mathrm{BAMS}_{ij} = \tfrac{1}{2}\left\{\tau_{ij}(\mu_{\mathrm{SLP}}) + \tau_{ij}(\sigma_{\mathrm{SLP}})\right\} \tag{7}$$

The representative year is then selected by requiring $\mathrm{BAMS}_{i,j}$ to be at a minimum for each month, i.e.

$$\mathrm{BAMS}_{\mathrm{RP},j} = \min_k\left\{\mathrm{BAMS}_{k,j}\right\} \tag{8}$$

2.2 Observational data base used for validation

The surface observational data employed here consist of wind speed and direction measurements from 22 automatic weather observation stations (ASOS) in *Comunidad Foral de Navarra*, Spain. These stations are managed and maintained by the *Sección de Evaluación de Recursos Agrarios del Departamento de Agricultura, Ganadería y Alimentación* at the regional Government of Navarra. Figure 1 shows their location together with the topography information which outline the complex topographic elements dominating the region: a complex system of mountain ranges in the centre, on the eastern and western side the mountain lines which form the last foothills of the Pyrenees to the north, and the less complex low lands of the Ebro valley which characterizes the south of the region. This figure also shows the position of the MERRA grid points over the area which is used for further analysis below.

Prior to the analyses related to the main topic of this paper the wind speed and wind direction records of the 22 stations were subjected to an extensive quality assurance analysis in order to remove both rough and systematic errors by using the methodology described in Chávez-Arroyo & Probst (2015). The data period from 1 January 2001 through 31 December 2012 was used for the purposes of the present work. The total data recovery after quality assurance was 94% global, with station data recovery ranging from 82% (NM20) to 98% (NM2) with a standard deviation of 5 percentage points.

2.3 Numerical data base

The Regional Weather Forecasting Model SKIRON was used to generate the numerical data set of surface wind speed employed in this study and includes 9 years of dynamically downscaled wind fields for the Iberian Peninsula for the period 2004-2012. The details of the SKIRON regional model are described in Kallos *et al.* (2005). Initial and boundary conditions were obtained from the NCEP Global Forecast System (GFS) global Numerical Weather Prediction model. Each SKIRON run is initialized as a cold start with the GFS analysis at 12 UTC of each day, and is run with a forecast horizon of 36 hours, updating the boundary conditions with GFS data every three hours. The first 12 hours are discarded as part of the spin-up time of the model (Gastón *et al.*, 2008) while the next 24 forecast hours are stored

every hour. These outputs are post-processed in order to obtain the wind speed at 80 m above surface from the native η vertical levels by performing a power-law interpolation to account for wind shear. The static data for representing vegetation, topography and soil texture are introduced at a resolution of 30", 30" and 2' respectively. In addition, a buffer zone of 100 km is considered by discarding this distance from the borders to avoid possible dynamical and numerical inconsistencies at the interface between the GFS and SKIRON boundaries.

2.4 The PCA and the SOM methods

The methods based on Principal Component Analysis (PCA) and Self-Organizing Maps (SOM) have been introduced by Chávez-Arroyo *et al.* (2013) and Chávez-Arroyo *et al.* (2015), respectively. As the BAMS method introduced in the present work both the PCA and the SOM method use mean sea level pressure maps from NCEP-DOE AMIP-II reanalysis (Kanamitsu *et al.*, 2002) as input. In the implementation of the PCA method the first Empirical Orthogonal Functions (EOFs) representing 70% of the variability were used. In the case of the SOM method, the number of nodes (C) used to describe the distribution function of the original data set was defined by three rectangular arrays with dimensions $[2 \times 3], [4 \times 5]$ and $[6 \times 6]$ equivalent to 6, 20 and 36 nodes, respectively. The reader is referred to the references above for a detailed description of both methods.

2.5 Implementations of the Rife method

The method described in Rife *et al.* (2013) requires data from a reanalysis location, taken to be the MERRA grid point closest to the point of interest in the original paper. A distance metric involving the squared differences between both the wind speed and wind direction distributions of the long-term and candidate representative year is used to determine the most representative (synthetic) year. Two versions of the Rife method (termed REA1 and REA2) were coded to allow for a fair comparison in the case of the validations against observational data (obtained from 22 met stations at the Navarra province). In the REA1 implementation the MERRA grid point showing the highest average correlation of the daily wind speed averages with all 22 Navarra ASOS data was selected; conversely, in the REA2 implementation the MERRA point with the lowest average correlation with all 22 Navarra weather stations was used.

As the Rife method in its original version was not designed to achieve mesoscale representativeness, a fair comparison called for an appropriate selection of the MERRA reference point to be used. Six locations on the Iberian Peninsula were selected randomly (shown in the inset of Figure 1) and the method was repeated for each of the reference points. The results of this sensitivity analysis are shown in Figure 6. While the reference point was found to have no statistically significant impact on the results, the results for two implementations (called R-I and R-II), chosen to be the ones with the "best" and "worst" error metrics, are shown below.

2.6 Validation metrics

The following metrics were calculated for each of the time series associated with each of the 22 weather stations (ASOS) at Navarra as well as each of the 99050 virtual wind speed records at 80 m above sea level obtained from the mesoscale model SKIRON. The first validation metric is the Relative Absolute Error (RAE) of a particular statistic such as the average ($x = \langle U \rangle$) or standard deviation ($x = \sigma(U)$) of the wind speed between the long-term (LT) and the representative (RP) time series:

$$|\varepsilon_x| = \left|\frac{x^{\mathrm{LT}} - x^{\mathrm{RP}}}{x^{\mathrm{LT}}}\right| \times 100\ [\%] \tag{9}$$

The second metric used for validation is the Mean Absolute Error (MAE) of either the hourly (T = 24 hours) or monthly (T = 12 months) wind speed time series averages:

$$|\varepsilon_T| = \frac{1}{T}\sum_{t=1}^{T}\left|U_t^{\mathrm{LT}} - U_t^{\mathrm{RP}}\right| \tag{10}$$

The third validation metric is the relative wind speed frequency difference

$$D = \sum_{g=1}^{\mathrm{nbins}} w_g \left|\frac{f_g^{\mathrm{LT}} - f_g^{\mathrm{RP}}}{f_g^{\mathrm{LT}}}\right| \times 100\ [\%] \tag{11}$$

where f_g^{LT} and f_g^{RP} are the relative wind speed frequencies corresponding to the long-term and representative period respectively, computed for a total number of bins given by nbins = 20. The weighting factor w_g is taken as the long-term frequency ($w_g = f_g^{\mathrm{LT}}$) in order to assign more importance to those bins with higher frequency of occurrence.

The last metric is based on the two-sample Kolmogorov-Smirnov (KS) test. This non-parametric hypothesis test evaluates the difference between the empirical cumulative wind speed distribution functions F of each pair of long-term and representative data sets (F_g^{LT} and F_g^{RP}). The KS metric is defined as

$$\mathrm{KS} = \max\left(\left|F^{\mathrm{LT}} - F^{\mathrm{RP}}\right|\right) \tag{12}$$

2.7 Analysis of statistical significance

In order to allow for a meaningful statistical comparison among the six methods described above a consistent procedure had to be devised to deal with the random structure associated with the Monte Carlo approach common to all methods. For this purpose, 100 realizations of each method were conducted, with each realization implying the generation of 10^5 trial cases, with the exception of the industry-standard or *traditional* method (TRA) which only generates one trial case. Subsequently, the results were subjected to a one-way ANOVA (Analysis of Variance) test (Wilks, 2006), as well as a non-parametric version, the Kruskal-Wallis (KW) test (Kruskal & Wallis, 1952). The Kruskal-Wallis test was run in addition to ANOVA as it had not been possible from the outset to ensure homoscedasticity (i.e. similar variance among group), a relatively stringent requirement for ANOVA. The KW test starts by ranking all data from all groups i together (in the present case, values of a given error metric for the different methods), ignoring group membership. The KW metric H then measures the deviation of the average group ranks $\bar{r}_i$ from the overall average rank $\bar{r}$ of the sample compared to the scatter of individual ranks r_{ij} of all data around $\bar{r}$, where j identifies data points within group i. A suitable p-value is defined in order to decide whether at least one group is significantly different from the others.

a. Each method was run 100 times and all error statistics (section 2.6) are gathered for either the Navarra ASOS or the mesoscale SKIRON wind field.

b. The average and the standard deviation of the error metrics of each trial were computed in the space dimension, i.e. for Q = 22 stations in the case of the Navarra ASOS network and for Q =

99050 SKIRON grid points in the case of the mesoscale simulations. One group (with 100 sample elements) was generated for each method.

c. Thereafter, a group comparison was conducted through the ANOVA test, in which the groups correspond to the six methods discussed above: BAMS, PCA, SOM, REA1, REA2, and TRA. The null hypothesis for the ANOVA is "the means for all the groups are equal", while the alternative hypothesis is "at least one mean is different". The hypotheses for the KW test are the same with the median instead of the mean. If the null hypothesis was rejected (p-value $\leq \alpha = 0.05$) in either the ANOVA or the KW test a Tukey-Kramer test (Tukey, 1949) was conducted in order to establish if the difference between any two of the means or medians (in the case of KW) was significant and to construct confidence limits (see e.g. (Hochberg & Tamhane, 1987) for a review of multiple comparison techniques). Tukey confidence limits are shown as bars in Figures 4, 5, 6, and 9.

The multiple trials of all methods were performed in identical manner for both data sets used for validation, i.e. the Navarra observational data and the numerical simulations conducted with SKIRON. The long-term reference periods are 1 January 2001 through 31 December 2012 (12 years) for the Navarra (ASOS) records and 1 January 2004 through 31 December 2012 (9 years) for the SKIRON-derived wind data.

3. Results and discussion

3.1 BAMS predictions for the Navarra network

The results of the BAMS method for a single run are illustrated in Figure 2; as in the following sections – with the exception of section 3.5 where the effect of the length of the representative period is assessed – the representative period is taken to be one year. Figure 2 (a) shows a histogram of the relative frequencies of the wind speed time series of both the long term and the best-matched representative year, together with their corresponding Weibull probability density functions (PDF). It is conspicuous that the PDF is very accurately predicted. Similarly, the daily profile (Figure 2 (b)) and the wind rose (Figure 2 (d)), two important metrics for annual energy production (AEP) estimate of wind farms, are almost identically reproduced by the representative. In the case of the seasonal profile (Figure 2 (c)) the majority of the monthly wind speeds are accurately predicted but occasional variations of up to 10% are also observed. It should be noted that at the ensemble level the BAMS actually predicts the seasonal profile consistently better than the other methods studied for comparison (see section 3.3).

3.2 BAMS predictions for the SKIRON mesoscale map of the Iberian Peninsula

Figure 3 shows the spatial distribution of the error of the wind speed average and energy density in the Iberian domain, obtained from one realization of the BAMS method. It can be noticed that, with the exception of a small area in the eastern part of the Iberian Peninsula, the wind speed error for most part of the domain is very low and homogeneous, with a mean of the map (i.e. mean of $\langle\varepsilon\rangle(U)$ for the 99050 time series) of 1.2% and a median of 0.9% for the absolute relative error of the wind speed prediction (left figure). Little dependence on geographic feature can be noticed in the map, which illustrates the robustness of the method. Given the cubic dependence of the wind energy density on wind speed the error in this variable is evidently higher, with an average error of 4% and a median of 3.1% compared to the long-term results, and the spatial variation is somewhat higher than in the case of the wind speed (right figure).

335 *3.3 Comparative performance of different methods*

336 (a) Kruskal-Wallis / ANOVA – Tukey-Kramer analysis for the Navarra network

337 A comparative study of the performance of the six methods discussed in this paper was conducted
338 according to the methodology described in section 2.7. As ANOVA has more stringent requirements
339 regarding the statistical properties of the groups of data to be compared (homoscedasticity, normality)
340 than the Kruskal-Wallis (KW) method, only the results obtained with the latter are shown for brevity.
341 However, it should be mentioned that the qualitative findings of the ANOVA approach (combined with
342 the Tukey-Kramer pairwise group comparison as in the KW case) are essentially identical to the ones
343 obtained with KW.

344 As shown in Figure 4 for the case of the Navarra met station network the p-value for the group
345 comparisons of all six metrics shown in the figure is $\ll 0.05$, so it can be safely stated that at least one of
346 the method is statistically different from the others. As illustrated by the Tukey-Kramer error bars the new
347 method (BAMS) and the two implementations of the Rife method all outperform the traditional method
348 (TRA) in a statistically significant sense for most of the error metrics but are indistinguishable among
349 each other. The PCA and SOM method, on the other hand, were found to be indistinguishable from the
350 TRA method in this study case. The Rife method, in its REA1 implementation, outperforms the PCA and
351 SOM methods in some of the metrics ($\varepsilon_{\langle U \rangle}$, ε_{24}, D, KS) while being indistinguishable from them in others
352 ($\varepsilon_{\sigma(U)}$, ε_{12}); the REA2 implementation is always indistinguishable from SOM and PCA. A noteworthy
353 feature is the fact the BAMS methods clearly outperforms all other methods in the case of the seasonal
354 profile (as measured by ε_{12}). We will see further below that this feature was also confirmed in the case of
355 the mesoscale simulations for the Iberian Peninsula. While the REA1 method is indistinguishable from
356 BAMS in five of the metrics and outperformed by BAMS in one (ε_{12}) it does show the lowest rank in
357 three of the metrics, insinuating a consistently good performance. It should be stated that this good result
358 can at least in part traced back to the fact that the MERRA reference used for the REA analysis was
359 selected within the region of the met stations against which the methods are validated, and that on top of
360 that the MERRA point with the highest average correlation with the Navarra network had been chosen.
361 This situation is somewhat different for the cases where the training region is different from the validation
362 region, as in the case of the mesoscale simulation discussed next.

363

364 (b) Kruskal-Wallis (KW) / ANOVA – Tukey-Kramer (TK) analysis for SKIRON mesoscale simulations

365 Evidently, validation of the different methods against mesoscale simulation is much more relevant to the
366 general topic of the present work (statistical-dynamical downscaling) than point comparisons, as the
367 rationale behind this approach is precisely the reduction of the computational effort required to perform a
368 long-term mesoscale simulation for a large area, such as the Iberian Peninsula. Figure 5 shows the results
369 obtained with the six methods.

370 It is clear from these graphs that in the case of the mesoscale simulation the new method (BAMS) now
371 dramatically outperforms all other methods. In all metrics BAMS has by far the lowest error ranks and is
372 clearly distinguishable (in a KW-TK sense) from all methods but the PCA approach which is statistically
373 indistinguishable in the case of three metrics, and the REA implementation R-I (the one providing the
374 best ranks in the KW method) whose TK error bounds overlap with those of BAMS in the case of $\varepsilon_{\sigma(U)}$.
375 Not unexpectedly, the runner-up to BAMS is also a mesoscale method, and the local method proposed by
376 Rife *et al.* (2013) (in its implementations R-I and R-II, the ones providing the best and worst ranks in the
377 KW analysis, respectively, out of the six implementations R1 through R6, see Figure 1) is not working as

well on a larger scale as on the local scale with data from the region which was used to train it in the first place. As seen from Figure 8 the REA implementations are now essentially indistinguishable from the traditional method (TRA) used for reference. It is interesting to note that the method based on a linear pattern analysis (PCA) is working somewhat better than its non-linear counterpart (SOM), which performs a complex (and computationally demanding) detection of non-linear patterns. This is of course a preliminary verdict, and other studies will have to show if this conclusion can be sustained on other data sets.

In order to treat the REA method in all fairness and to avoid that the selection of the reference point used for training of the method would unduly influence the results, six versions were implemented where the reference point was changed to six random locations (R1 through R6) distributed evenly over the Iberian Peninsula (Figure 1). The results are shown in Figure 6, where both a boxplot for the individual results (providing error statistics for the 99050 locations/time series of the SKIRON mesoscale wind map) and a group comparison plot have been provided. For brevity, only the metrics D (measuring wind speed probability distributions) and $\varepsilon_{\langle U \rangle}$ (measuring the global error in the wind speed prediction) have been shown. ANOVA/Tukey-Kramer results are shown, but as in the previous cases, the Kruskal-Wallis analysis provided essentially the same results. It can be seen from the figure that the results obtained with either of the REA implementation were found to be statistically indistinguishable in an ANOVA sense, as indicated by the high value of the p-value (0.72 and 0.84, respectively) and the overlap of the TK error bounds. This is of course not all that surprising as in a local method like REA an increase in accuracy in one location (the training location) is likely to come at the expense of a lesser accuracy in the rest of the simulation region, resulting in a similar overall error. It has of course to be recognized that the REA was not originally designed for mesoscale assessments for regions as large as the Iberian Peninsula, and that the extension of it by the authors of the present work was for reference purposes only.

3.4 Repeatability of the methods

In order to obtain further insights into repeatability of the results the variance for each of the annual ensemble average wind speed values of the 99050 locations modelled in the SKIRON mesh was calculated, where - as before - the ensemble consisted of $M = 100$ realizations of each method. The results are shown in Figure 7 as maps of the wind speed variance for each method. It is conspicuous from the colour scales of the maps that the traditional method by far has the largest variability among realizations and that the latter is relatively uniform over the simulation region, with the exception of a few regions of higher variability in the mountain ranges in North-eastern Spain. This results was somewhat expected, given the simple design of the method. On the other end of the range, the BAMS method is again seen to outperform all other methods in terms of its high repeatability and a very high homogeneity, i.e. very low dependence of the variability on location. It therefore provided what is expected from a model suitable for mesoscale modelling. The runner-up, as before, as the PCA-based method which shows a total variance only some 10% higher than BAMS and also a relatively good spatial homogeneity. SOM and REA1 have a similar total variance and spatial homogeneity over the continental part of the simulation domain, though REA1 shows a higher variability over the seas, particular the Atlantic Ocean adjacent to Portugal and Galicia (North-western Spain).

3.5 The role of the length of the representative period

While it is intuitive to assume that a representative year should be the natural choice for the representative (synthetic) period of a long-term period to be simulated under a mesoscale approach, it can also be expected that there will be cost-benefit trade-off which has to be assessed for an optimal use of

computational resources while ensuring accuracy. Periods significantly shorter than one year are prone to create biases associated with a lack of seasonal representativeness. Periods composed of several years might be able to better assess inter-annual fluctuations but come at a higher computational cost. Figure 8 has the evolution of four error metrics as a function of the duration of the representative period; note the non-linear time axis. It is evident from the figure that a consistent reduction both in average and in variability among Monte Carlo realizations occurs as the length of the synthetic period is increased.

A power law was found to be a very good fit ($R^2 > 0.99$) to all four metrics shown in Figure 8, with power law exponents in the range of -0.57 (for $\varepsilon_{\langle U \rangle}$) to -0.77 (for $|\varepsilon_{12}|$), indicating that the seasonal profile benefits most from an extension of the representative period which is of course very intuitive. In can be seen from Figure 8 that the average absolute error of the average wind speed $\langle U \rangle$ (i.e. $\varepsilon_{\langle U \rangle}$) is of the order of 1.5% for a one-year representative period, down from about 6% if a 36-day period is chosen. Using two years as a representative period provides only a marginal improvement to about 1%.

While Figure 9 strongly suggests a significant improvement in long-term prediction accuracy as a function of the length of the representative period it still remained to be assessed to what extent these improvements are significant in a statistical sense. In order to address this question another round of Kruskall-Wallis (KW) non-parametric group comparisons was conducted where each group consisted of the long-term predictions elaborated with representative periods (RP) of varying length (as before) and a given error metric. As shown by the results in KW ranks do indeed decline consistently as a function of the RP length, increasing the RP length not always guarantees a significant improvement in prediction accuracy, e.g. upon increasing the RP length from 120 to 180 days. However, it is evident from the figure that the expected error in a given error metric can be tuned by selecting the appropriate length of the representative period.

In order to further elaborate on this aspect, which directly translates into the computational effort required to achieve a given level of accuracy, an attempt was made to directly relate the BAMS scores (as calculated by equation (7)) with the expected accuracy of the (SKIRON) mesoscale simulation conducted with the reduced synthetic period instead of the full long-term period. Figure 10 shows the corresponding results. It can be seen that in all six error metrics shown the relationship between the error and the BAMS scores is approximately linear, allowing the level of computational effort (length of the period to be simulated) to be adjusted to the level of final accuracy required. Evidently, a reduction of the error associated with the selection of the synthetic period is only worthwhile to the extent that this error is larger than or comparable to other sources of errors associated with the mesoscale modelling process.

3.6 Savings in computational resources

In an effort to quantify the computational cost of the main contribution of the present work, the BAMS method, was run for the Iberian domain on an Intel Xeon processor (using a single core@2.53GHz), requiring 38 hours of execution. However, as the method can be fully parallelized the same task using the full 12-core set of the processor would require less than four hours. With this computational investment the required execution time of a downscaling process for the same domain can be reduced by a factor of 20 to 30 (depending on the exact lengths of both the representative and the required long-term period). This translates into a speedup in a cloud computing environment from typically one month to little over one day, saving both considerable amounts of financial resources and allowing for a greater range of sensitivity studies.

4. Summary and conclusions

A new method for the statistical-dynamical downscaling of the resource, termed the BAMS method (*Best Annual Mean and Standard Deviation*), has been introduced. This method allows to construct a synthetic representative period with an optimal similarity compared to a long-term period of interest; this reduced period can then be used for dynamical downscaling purposes at a fraction of the time that would have been required if the long-term period had been downscaled directly. The BAMS method is an algorithmic approach which does not require specific knowledge about the wind climate in the region of interest, as opposed to statistical-dynamical downscaling methods based on classifications of wind resource data prior to the construction of the representative data set. It has the distinctive advantage over other algorithmic methods that it does not require the specification of *a priori* information such as a number of retained orthogonal components (as in the case of *Principal Component Analysis*) or prior selection of the number and structure of cluster arrays (as in the case of *Self-Organizing Maps*). Much as many algorithmic but unlike most classification-based methods BAMS retains control of the temporality of the data which is very important in the case of wind resource studies where seasonal and daily profiles are of great interest. The BAMS method is based on the use of mesoscale input information, in the present case mean sea level pressure (MSLP) maps, which allow for the construction of a regionally representative period rather than one tuned to a specific site of interest. It was shown that the new method clearly outperforms the other methods in all error metrics studied, indicative of different characteristics of the wind resource. Even with the continuous rise in computing power available to general and research users long-term mesoscale simulation remain a significant computational challenge, and it is believed that the approach presented in the current work significantly contributes to the progress of the field.

Acknowledgements

Support from Tecnológico de Monterrey through the Energy and Climate Change group, as well as a tuition stipend for one of the authors (R.Ch.) is greatly acknowledged. R.Ch. also appreciates ample support from CONACYT (Mexico) for a Ph.D. scholarship and his research year abroad through the *Becas Mixtas* fund. One of the authors (J.A.) acknowledges the support of the UK National Centre for Earth Observation (NCEO).

References

Barranger N., Kallos G. 2012. The use of an atmospheric model to solve wind forcing turbulent flows over complex terrain for wind resource assessment. In: *EMS general assembly*. Łódź,.

Castro CL. 2005. Dynamical downscaling: Assessment of value retained and added using the Regional Atmospheric Modeling System (RAMS). *J. Geophys. Res.* **110**:1–21.

Chávez-Arroyo R., Lozano-Galiana S., Sanz-Rodrigo J., Probst O. 2013. On the Application of Principal Component Analysis for Accurate Statistical-dynamical Downscaling of Wind Fields. *Energy Procedia* **40**:67–76.

Chávez-Arroyo R., Lozano-Galiana S., Sanz-Rodrigo J., Probst O. 2015. Statistical-dynamical downscaling of wind fields using self-organizing maps. *Appl. Therm. Eng.* **75**:1201–1209.

Chávez-Arroyo R., Probst O. 2015. Quality assurance of near-surface wind velocity measurements in Mexico. *Meteorol. Appl.* **22**:165–177.

Cutler NJ., Jorgensen BH., Ersboll BK., Badger J. 2006. Class generation for numerical wind atlases. *Wind Eng.* **30**:401–415.

503 Frank HP., Landberg L. 1997. Modeling the wind climate of Ireland. *Bound. Lay. Meteorol.* **85**:359–378.

504 Frey-Buness F., Heimann D., Sausen R. 1995. A Statistical-Dynamical Downscaling Procedure for
505 Global Climate Simulations. *Theor. Appl. Clim.* **50**:117–131.

506 Fuentes U., Heimann D. 2000a. An Improved Statistical-Dynamical Downscaling Scheme and its
507 Application to the Alpine Precipitation Climatology. *Theor. Appl. Clim.* **65**:119–135.

508 Fuentes U., Heimann D. 2000b. An Improved Statistical-Dynamical Downscaling Scheme and its
509 Application to the Alpine Precipitation Climatology. *Theor. Appl. Clim.* **65**:119–135.

510 García-Bustamante E., González-Rouco JF., Navarro J., Xoplaki E., Jiménez P a., Montávez JP. 2012.
511 North Atlantic atmospheric circulation and surface wind in the Northeast of the Iberian Peninsula:
512 uncertainty and long term downscaled variability. *Clim. Dyn.* **38**:141–160.

513 Gastón M., Pascal E., Frías L., Martí I., Irigoyen U., Cantero E., Sergio L., Loureiro Y. 2008. Wind
514 resources map of Spain at mesoscale . Methodology and validation on. In: *European Wind Energy*
515 *Conference and Exhibition*. Brussels, Belgium,.

516 Hagemann K. 2008. Mesoscale Wind Atlas of South Africa. University of Cape Town.

517 Hahmann AN., Lange J., Peña A., Hasager CB. 2012. *The NORSEWInD numerical wind atlas for the*
518 *South Baltic*. Roskilde, Denmark.

519 Hochberg Y., Tamhane AC. 1987. *Multiple Comparison Procedures*. NJ: John Wiley & Sons, Inc.

520 Kallos G., Katsafados P., Papadopoulos A. 2005. *The Weather Forecasting System SKIRON - Description*
521 *of the model*. Athens, Greece.

522 Kanamitsu M., Ebisuzaki W., Woollen J., Yang S-K., Hnilo JJ., Fiorino M., Potter GL. 2002. NCEP–
523 DOE AMIP-II Reanalysis (R-2). *B. Am. Meteorol. Soc.* **83**:1631–1643.

524 Kruskal WH., Wallis WA. 1952. Use of Ranks in One-Criterion Variance Analysis. *J. Am. Stat. Assoc.*
525 **47**:583–621.

526 Liléo S., Berge E., Undheim O., Klinkert R., Bredesen RE. 2013. Long-term correction of wind
527 measurements. State-of-the-art, guidelines and future work. In: *EWEA*. 1–10.

528 Martinez Y., Yu W., Lin H. 2013. A new Statistical–Dynamical Downscaling procedure based on EOF
529 analysis for regional time series generation. *J. Appl. Meteor. Clim.* **52**:935–952.

530 Mesinger F., DiMego G., Kalnay E., Mitchell K., Shafran PC., Ebisuzaki W., Jović D., Woollen J.,
531 Rogers E., Berbery EH., Ek MB., Fan Y., Grumbine R., Higgins W., Li H., Lin Y., Manikin G.,
532 Parrish D., Shi W. 2006. North American Regional Reanalysis. *Bull. Am. Meteorol. Soc.* **87**:343–
533 360.

534 Pielke RAS. 2002. *Mesoscale Meteorological Modeling*. Academic Press.

535 Rienecker MM., Suarez MJ., Gelaro R., Todling R., Bacmeister J., Liu E., Bosilovich MG., Schubert SD.,
536 Takacs L., Kim G., Bloom S., Chen J., Collins D., Conaty A., da Silva A., Gu W., Joiner J., Koster
537 RD., Lucchesi R., Molod A., Owens T., Pawson S., Pegion P., Redder CR., Reichle R., Robertson
538 F., Ruddick A., Sienkiewicz M., Woollen J. 2011. MERRA - NASA's Modern-Era Retrospective
539 Analysis for Research and Applications. *J. Clim.* **24**:1–41.

Rife DL., Vanvyve E., Pinto JO., Monaghan AJ., Davis CA., Poulos GS. 2013. Selecting representative days for more efficient dynamical climate downscaling: Application to wind energy. *J. Appl. Meteorol. Climatol.* **52**:47–63.

Romo Perea A., Amezcua J., Probst O. 2011. Validation of three new measure-correlate-predict models for the long-term prospection of the wind resource. *J. Renew. Sustain. Energy* **3**:23105.

Tammelin B., Vihma T., Atlaskin E., Badger J., Fortelius C., Gregow H., Horttanainen M., Hyvönen R., Kilpinen J., Latikka J. 2013. Production of the Finnish Wind Atlas. *Wind Energy* **16**:19–35.

Tukey JW. 1949. Comparing Individual Means in the Analysis of Variance. *Biometrics* **5**:99–114.

Vanvyve E., Delle Monache L., Monaghan AJ., Pinto JO. 2015. Wind resource estimates with an analog ensemble approach. *Renew. Energy* **74**:761–773.

Wang Z., Bovik AC., Sheikh HR., Simoncelli EP. 2004. Image quality assessment: From error visibility to structural similarity. *IEEE Trans. Image Process.* **13**:600–612.

Wilks DS. 2006. Statistical Methods in the Atmospheric Sciences. *Int. Geophys. Ser.* **102**:380–380.

Figure captions

Figure 1 Location of the ASOS stations used in the present work. The MERRA reference locations REA1 and REA2 for the REA method in the case of the local validation are indicated in the main graph. *Inset:* Locations of the reference locations R1 through R6 used for the REA method in the case of the mesoscale validation.

Figure 2 Comparison of the basic wind statistics for the long-term period (LT) and the representative year (RY) determined by one realization of the BAMS method for one ASOS (NM19) from the Navarra network. (a) Histograms of the wind speed distributions, (b) daily profiles, (c) seasonal profiles, and (d) wind roses.

Figure 3 (a) Absolute wind speed error for one realization of the BAMS method. (b) Absolute error of the wind energy density.

Figure 4 Results of the Kruskal-Wallis / Tukey-Kramer pairwise group comparison for the six methods under study using the Navarra observational data for validation

Figure 5 Results of the Kruskal-Wallis / Tukey-Kramer pairwise group comparison for the six methods under study using the SKIRON mesoscale data for the Iberian Peninsula for validation

Figure 6 Results of the ANOVA / Tukey-Kramer pairwise group comparison for six implementations of the REA method

Figure 7 Maps of the variance of the wind speed of the representative year obtained from M=100 realizations of each method

Figure 8 Box-plots with several error statistics as a function of the length of the synthetic period selected for the case of the BAMS method. Each sample in the plots is built with the average of results obtained at the 99050 SKIRON grid points of each metric. Red asterisks denote the mean of each error metric over the 100 trials. Green circles (with corresponding vertical axis on the right of each plot) denote the standard deviation of the trials.

Figure 9 Results of the multiple comparisons test (Kruskall-Wallis / Turkey-Kramer) for SKIRON-derived wind fields and different length of the representative period selected through the BAMS method. Each metric include their mean and their narrow confidence intervals for the join significance (with $\alpha = 0.05$) constructed from the Kruskall-Wallis results.

Figure 10 Correlation between the BAMS scores and six different error metrics for the case of the SKIRON mesoscale simulations

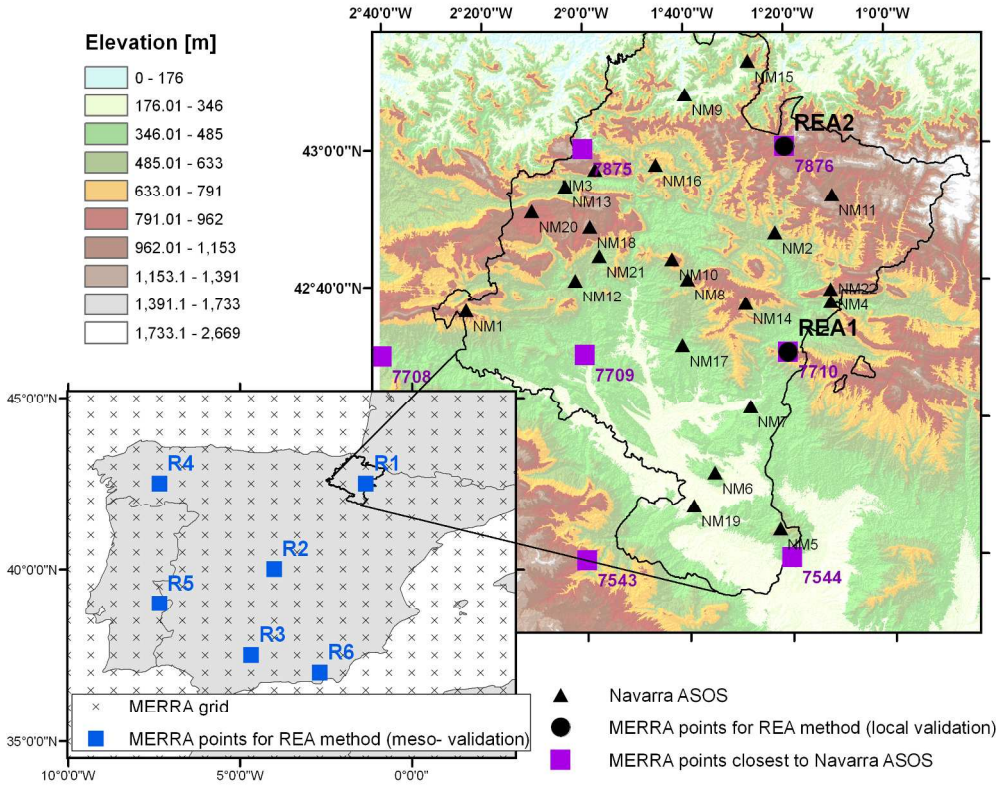

Figure 1 Location of the ASOS stations used in the present work. The MERRA reference locations REA1 and REA2 for the REA method in the case of the local validation are indicated in the main graph. Inset: Locations of the reference locations R1 through R6 used for the REA method in the case of the mesoscale validation.
Figure 1
215x177mm (300 x 300 DPI)

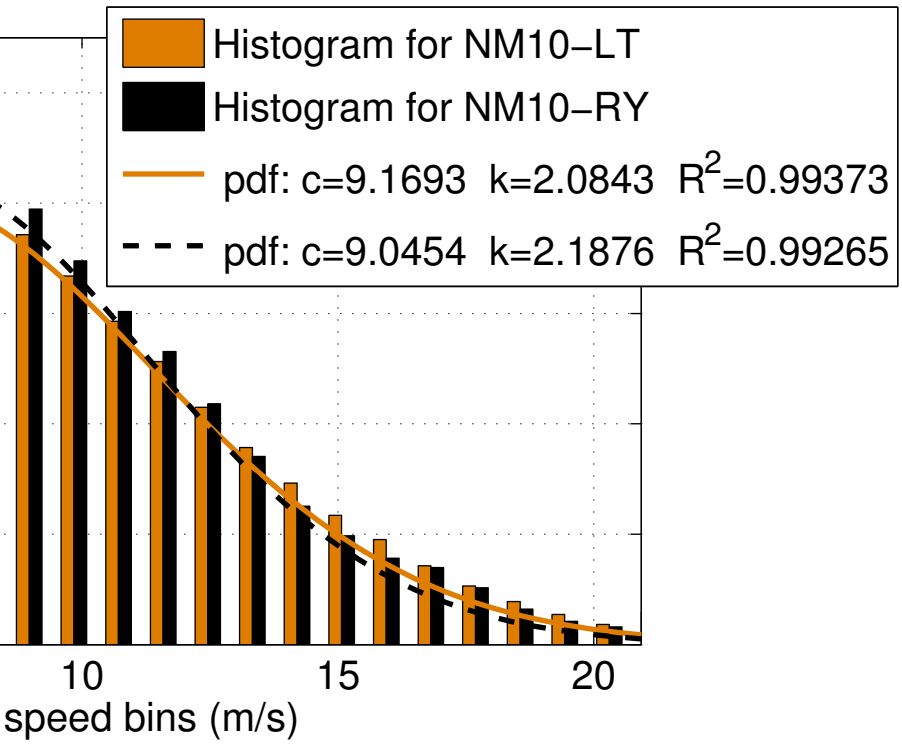
Histogram for NM10−LT
Histogram for NM10−RY
pdf: c=9.1693 k=2.0843 R2=0.99373
pdf: c=9.0454 k=2.1876 R2=0.99265
10
15
20
speed bins (m/s)

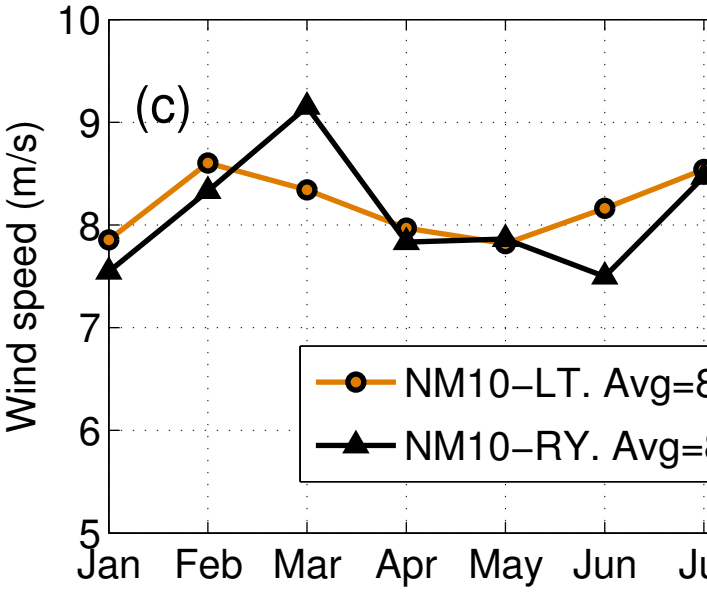
(c)
Wind speed (m/s)
10
9
8
7
6
5
Jan
Feb
Mar
Apr
May
Jun
NM10−LT. Avg=
NM10−RY. Avg=

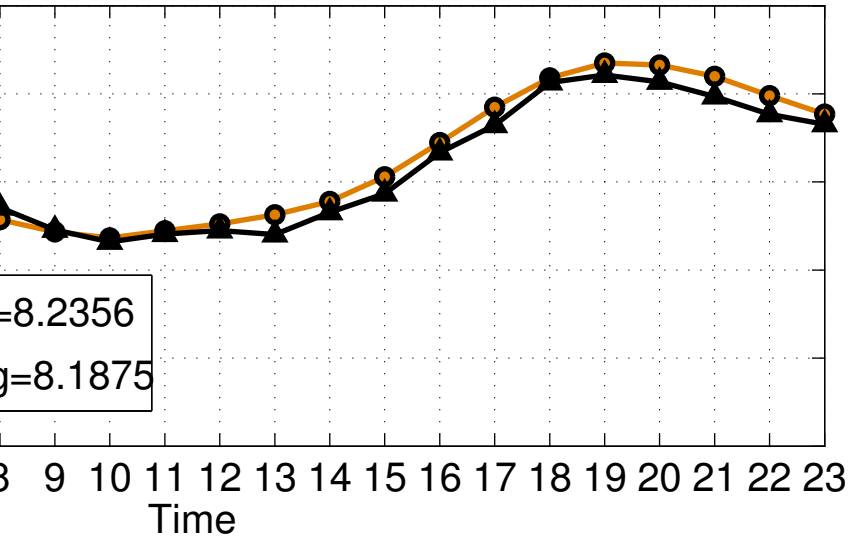
=8.2356
g=8.1875
3 9 10 11 12 13 14 15 16 17 18 19 20 21 22 23
Time

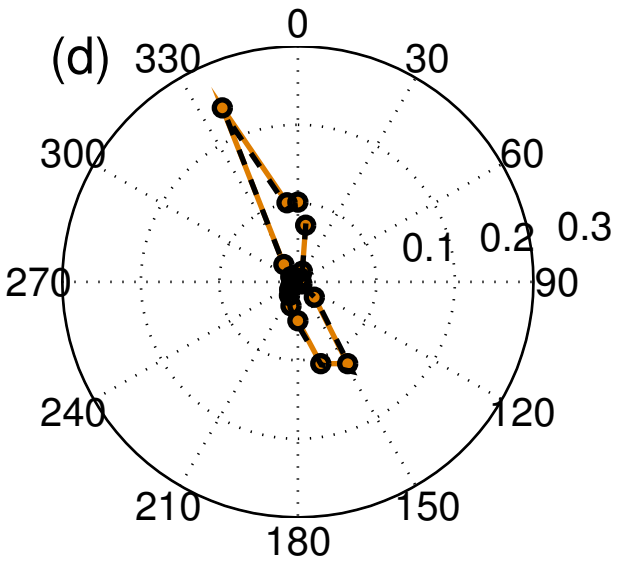
(d)
0
30
60
90
120
150
180
210
240
270
300
330
0.1
0.2
0.3

peed absolute error, $\varepsilon_{<U>}$ (%)

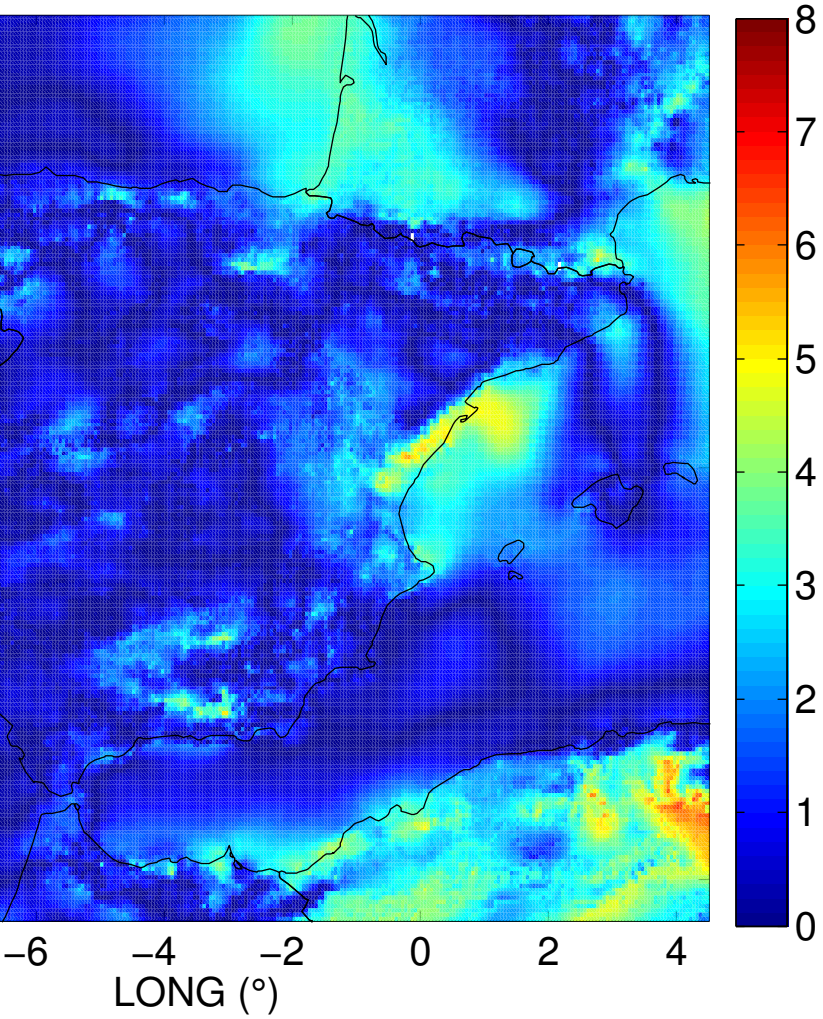

Energy density absolut

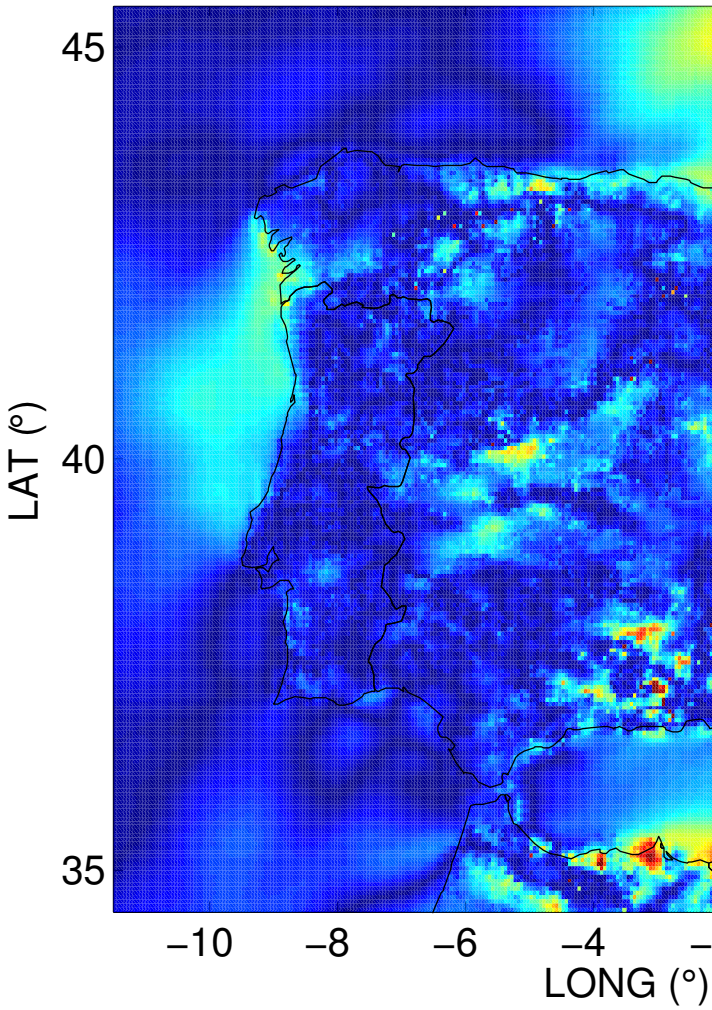

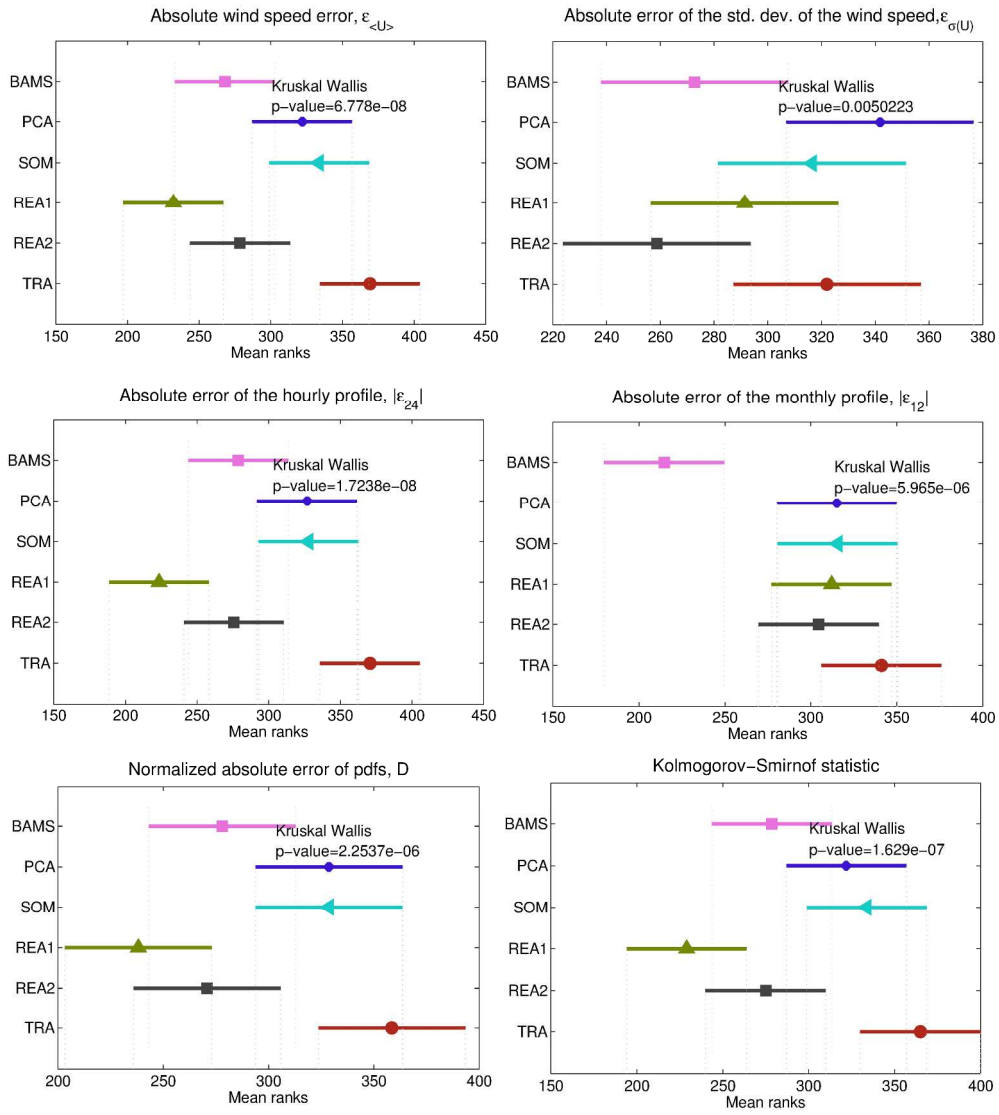

Figure 4 Results of the Kruskal-Wallis / Tukey-Kramer pairwise group comparison for the six methods under study using the Navarra observational data for validation

Figure 4
360x402mm (300 x 300 DPI)

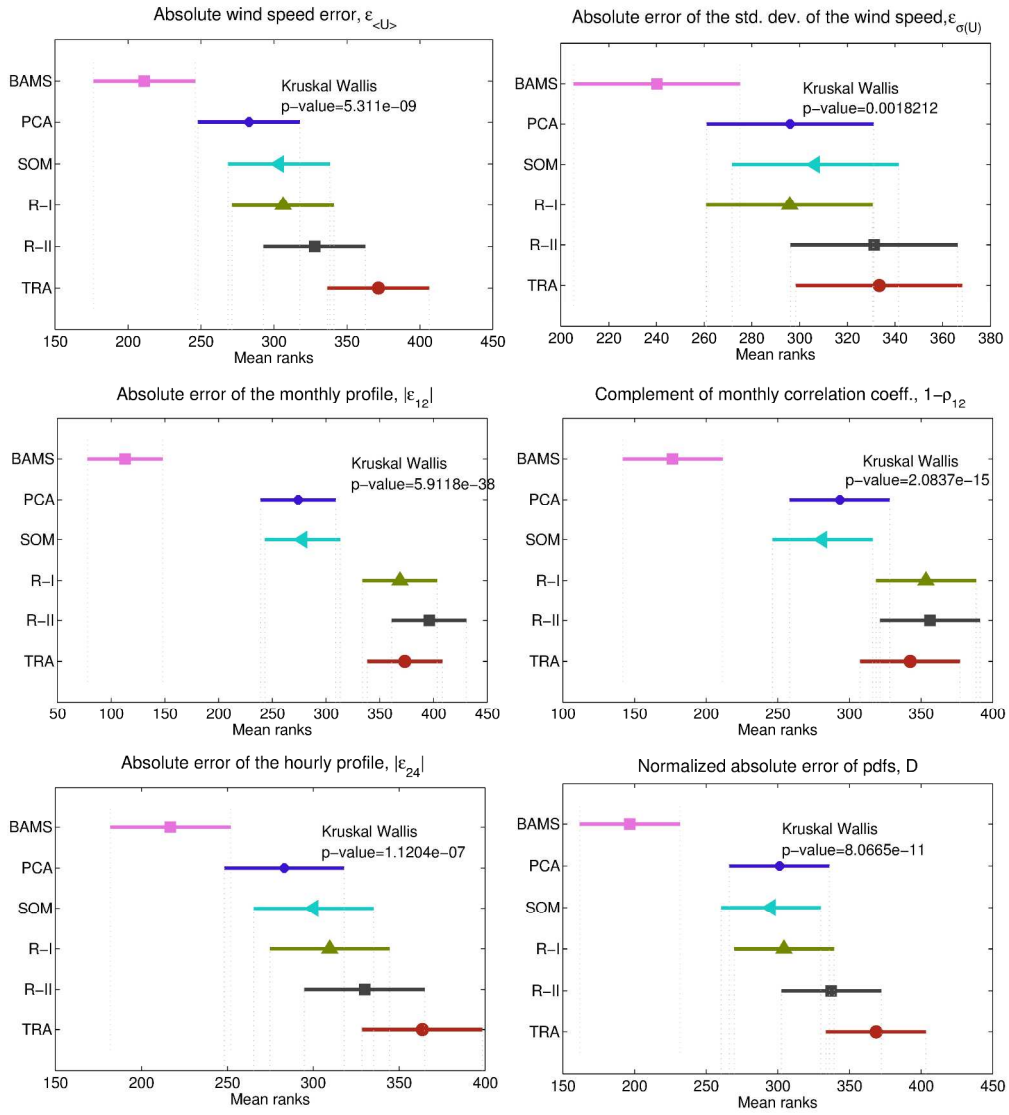

Figure 5 Results of the Kruskal-Wallis / Tukey-Kramer pairwise group comparison for the six methods under study using the SKIRON mesoscale data for the Iberian Peninsula for validation
Figure 5
360x402mm (300 x 300 DPI)

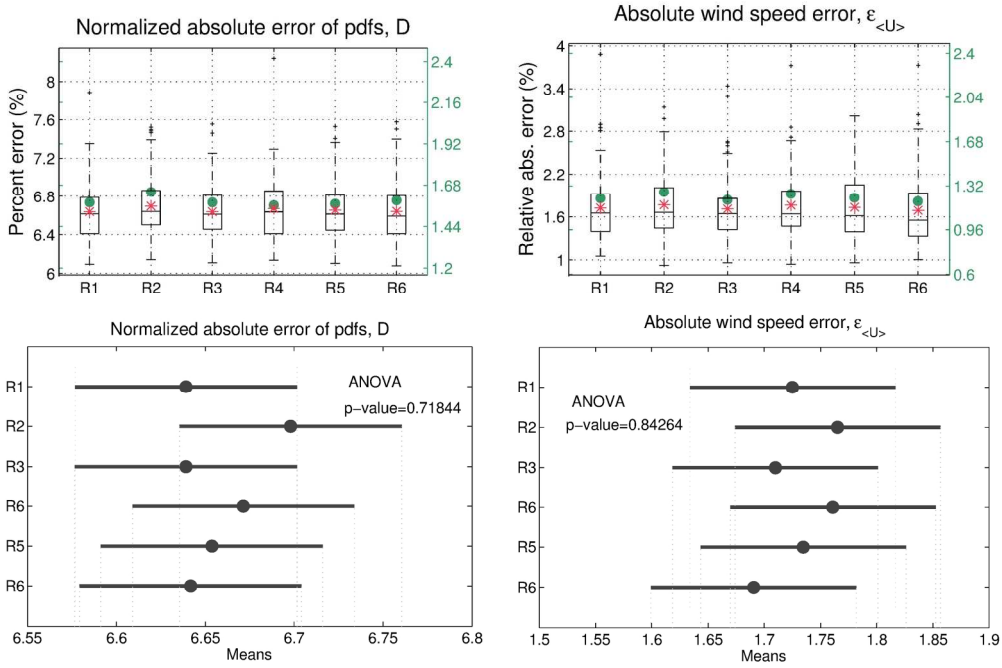

Figure 6 Results of the ANOVA / Tukey-Kramer pairwise group comparison for six implementations of the REA method
Figure 6
187x129mm (300 x 300 DPI)

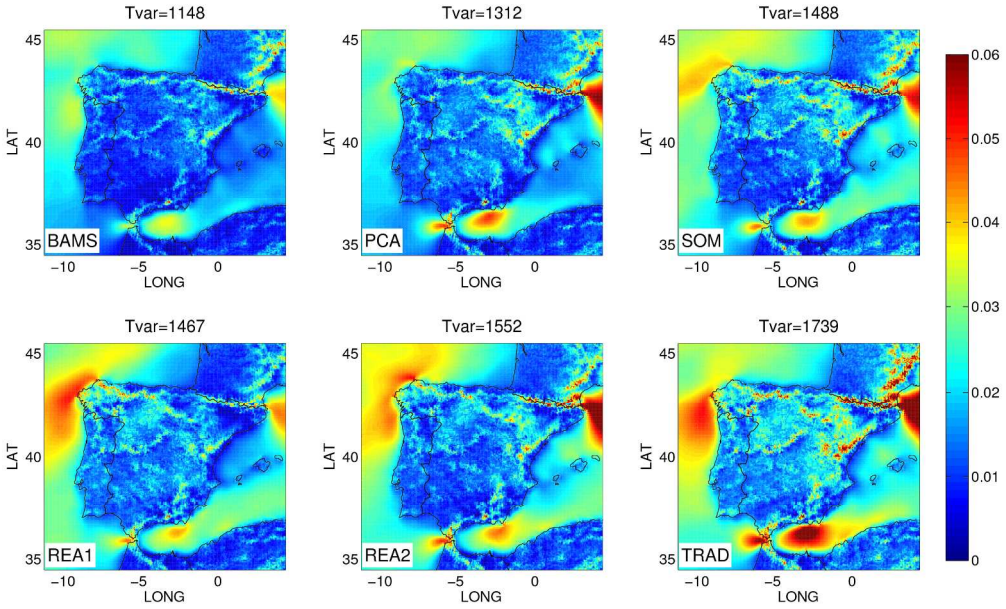

Maps of the variance of the wind speed of the representative year obtained from M=100 realizations of each method
Figure 7
706x433mm (96 x 96 DPI)

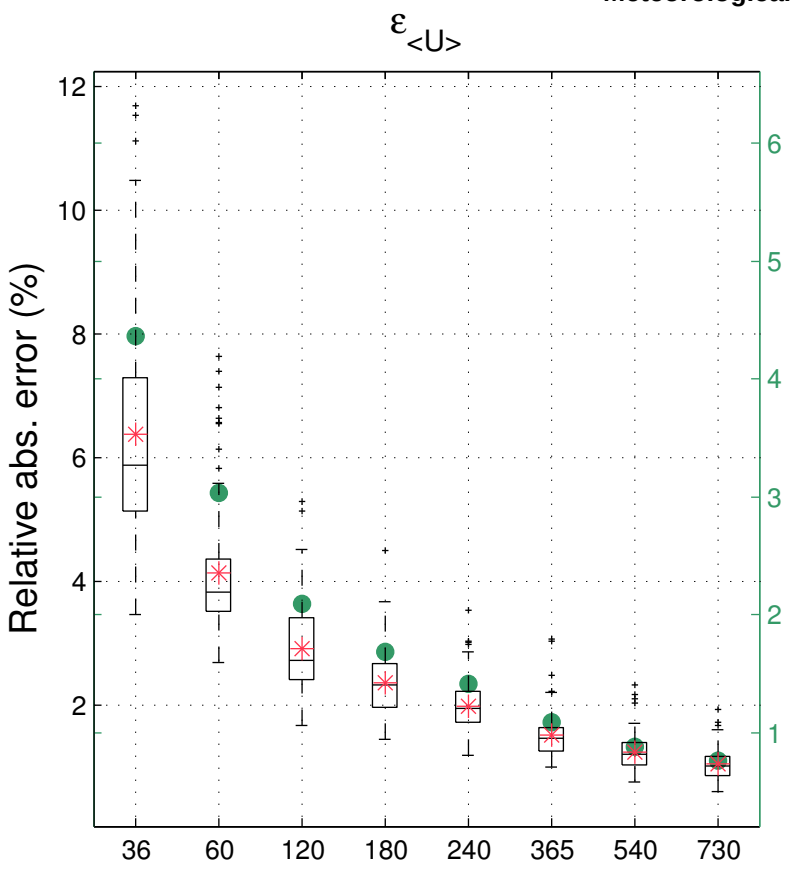
ε<U>
Relative abs. error (%)
12
10
8
6
4
2
6
5
4
3
2
1
36 60 120 180 240 365 540 730

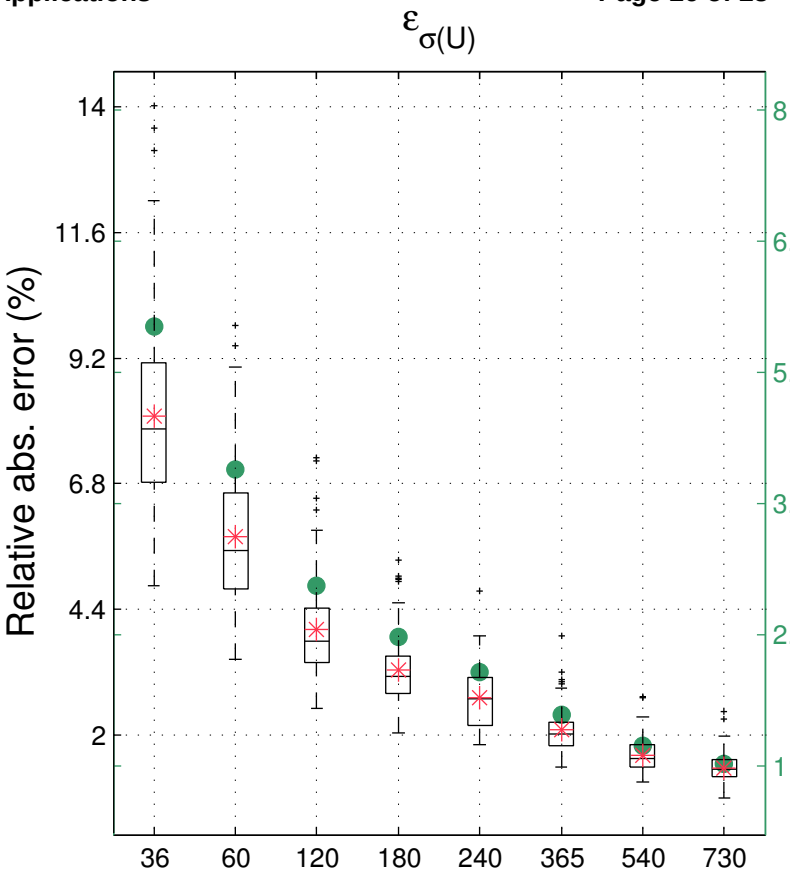
ε σ(U)
Relative abs. error (%)
14
11.6
9.2
6.8
4.4
2
8
6
5
3
2
1
36 60 120 180 240 365 540 730

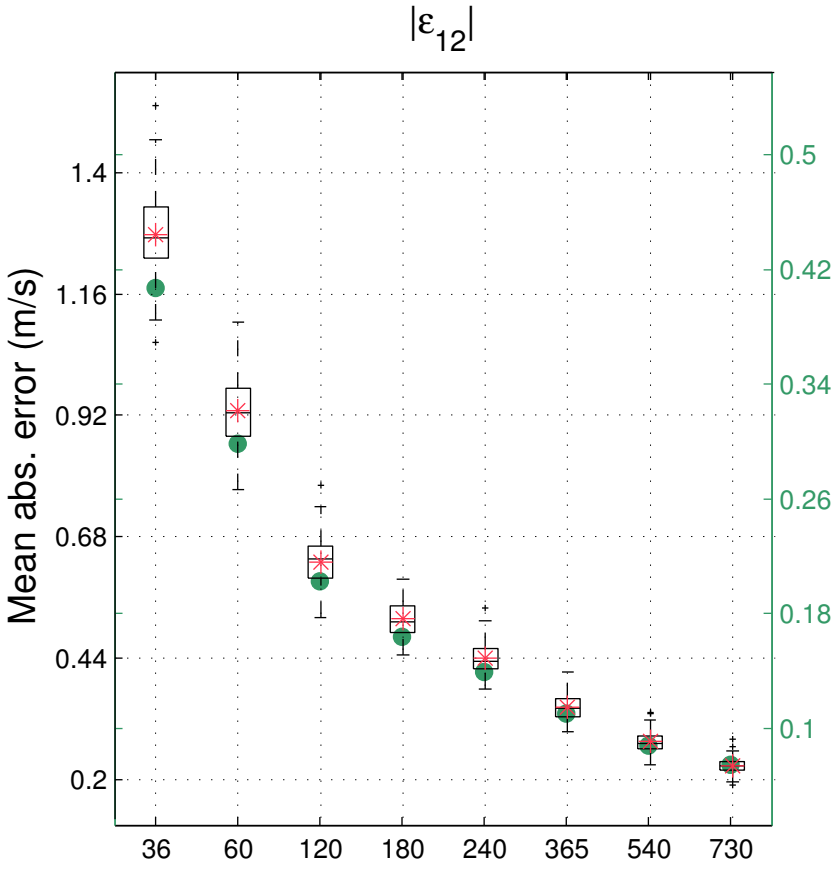
|ε12|
Mean abs. error (m/s)
1.4
1.16
0.92
0.68
0.44
0.2
0.5
0.42
0.34
0.26
0.18
0.1
36 60 120 180 240 365 540 730

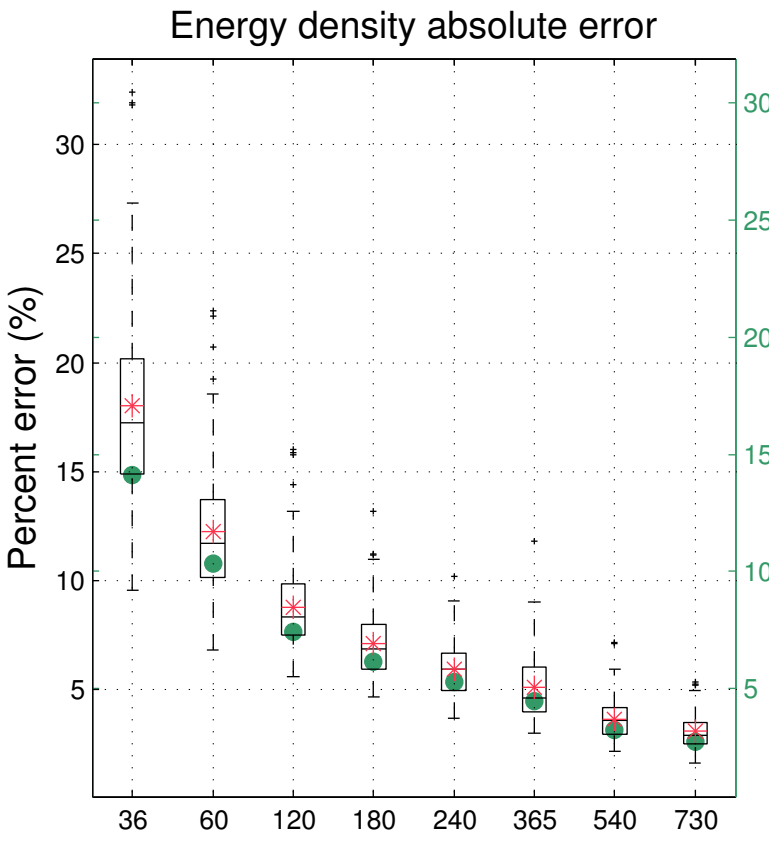
Energy density absolute error
Percent error (%)
30
25
20
15
10
5
30
25
20
15
10
5
36 60 120 180 240 365 540 730

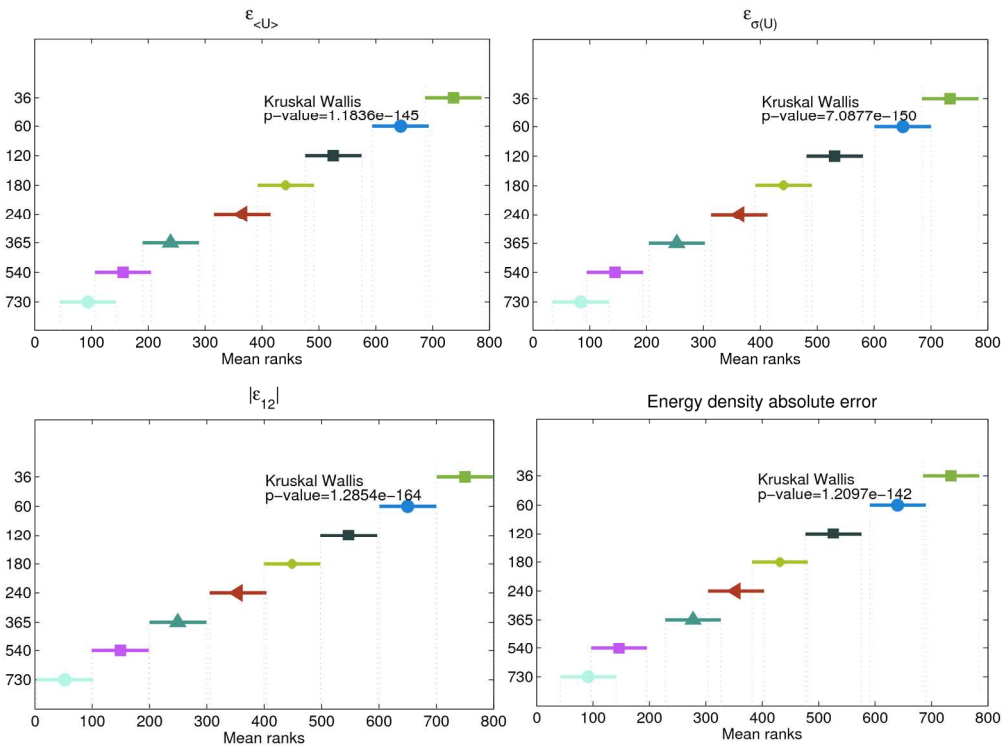

Results of the multiple comparisons test (Kruskall-Wallis / Turkey-Kramer) for SKIRON-derived wind fields and different length of the representative period selected through the BAMS method. Each metric include their mean and their narrow confidence intervals for the join significance (with α= 0.05) constructed from the Kruskall-Wallis results

Figure 9

675x500mm (96 x 96 DPI)

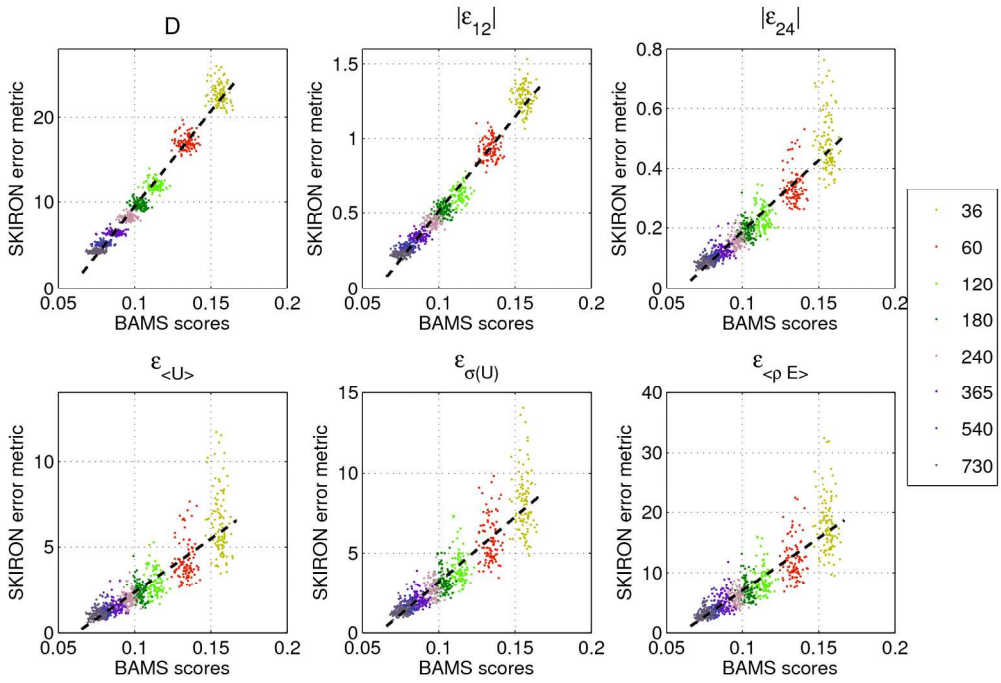

Correlation between the BAMS scores and six different error metrics for the case of the SKIRON mesoscale simulations
Figure 10
540x372mm (96 x 96 DPI)